

Directed Emission from Self-Assembled Microhelices

Lukas Helmbrecht, Melissa Tan, Ruslan Röhrich, Marloes H. Bistervels, Bruno Ortiz Kessels, A. Femius Koenderink, Bart Kahr, and Willem L. Noorduin*

Bottom-up assembly can organize simple building blocks into complex architectures for light manipulation. The optical properties of self-assembled polycrystalline barium carbonate/silica double helices are studied using fluorescent Fourier and Mueller matrix microscopy. Helices doped with fluorescein direct light emission along the long axis of the structure. Furthermore, light transmission measured normal and parallel to the long axis exhibits twist sense-specific circular retardance and waveguiding, respectively, although the measurements suffer from depolarization. The helices thus integrate highly directional emission with enantiomorph-specific polarization. This optical response emerges from the arrangement of nanoscopic mineral crystallites in the microscopic helix, and demonstrates how bottom-up assembly can achieve ordering across multiple length scales to form complex functional materials.

1. Introduction

Material syntheses based on self-assembly have given rise to structures with unique mechanical, magnetic, electric, and optical properties.^[1–6] Such bottom-up assembly strategies also enable hierarchical ordering of building blocks across multiple length scales, thereby offering the opportunity to integrate multiple functionalities within a single material.

Helical-shaped nanocomposites formed from barium carbonate (BaCO_3) nanocrystals and amorphous silica (SiO_2) can put these ideas to the test. These bioinspired nanocomposites have been observed to self-assemble into highly intricate, yet controllable, 3D shapes such as vases, stems, and helices, that can be further sculpted and chemically modified.^[7–18] The structural layout of the helical composites has been studied in great detail: the rod-shaped nanocrystals are elongated along their c -axes and align parallel to one another while precessing

tangentially around the helical axis,^[8–18] thus forming a chiral ensemble, as shown in Figure 1.

It is well-known that chiral assemblies of achiral building blocks can exhibit handedness-specific optical responses.^[19,20] Hence, the intricately ordered, anisotropic medium of the helices suggests that these architectures may have optical properties absent in their building blocks alone. The twisting matrix overlays linearly birefringent nanocrystals of BaCO_3 ($n_\alpha = 1.529$, $n_\beta = 1.676$, $n_\gamma = 1.677$) in multiple directions with respect to incident wave vectors.^[21,22] Moreover, the high refractive indices of the $\text{BaCO}_3/\text{SiO}_2$ ($n \approx 1.5$) medium may also affect total internal reflection and waveguiding at

some optical frequencies.^[13,23] These expectations are evaluated by studying the optical properties of helices using fluorescent Fourier microscopy and Mueller matrix microscopy.^[24,25]

2. Results and Discussion

2.1. Analyzing Directed Emission

$\text{BaCO}_3/\text{SiO}_2$ helices were synthesized according to a previously developed coprecipitation reaction (see the Experimental Section for details).^[14] After growth of 1.5 h, typical helices were $\approx 40 \mu\text{m}$ long and $5 \mu\text{m}$ wide with a pitch of about $10 \mu\text{m}$. Fluorescein was incorporated during growth to enable active light emission.^[13] If a helix behaves as a waveguide, scattered light within should be directed to the tip. We investigated the directional emission of individual helices with respect to their orientation, characterized by a polar tilt and azimuthal rotation (Θ_{H} and Φ_{H} , respectively) relative to a glass cover slip substrate (Figure 2). These angles can be measured directly by scanning electron microscopy (SEM) (see Section S2 in the Supporting Information).

The direction of emitted light was determined using a home-built Fourier or k -space microscope (Figure 2a and Section S1 (Supporting Information)).^[26] The base of the helix was excited with a laser ($\lambda = 490 \text{ nm}$). The emission ($\lambda_{\text{E}} = 510 \text{ nm}$) was collected with a high numerical aperture objective ($\text{NA} = 0.9$), whose back focal plane (Fourier plane) was projected onto a camera detector, where each pixel position in the image corresponds to an angle of incident light in real space (Figure 2a,c). Isotropic emission would give a diffuse Fourier image, whereas directed emission would produce a focused spot.

L. Helmbrecht, R. Röhrich, M. H. Bistervels, B. O. Kessels, Prof. A. F. Koenderink, Dr. W. L. Noorduin
AMOLF

Science Park 104, 1098XG Amsterdam, The Netherlands
E-mail: noorduin@amolf.nl

M. Tan, Prof. B. Kahr
Department of Chemistry
New York University
100 Washington Square East, New York City, NY 10003-6688, USA

R. Röhrich
ARCNL
Science Park 106, 1098XG Amsterdam, The Netherlands

 The ORCID identification number(s) for the author(s) of this article can be found under <https://doi.org/10.1002/adfm.201908218>.

DOI: 10.1002/adfm.201908218

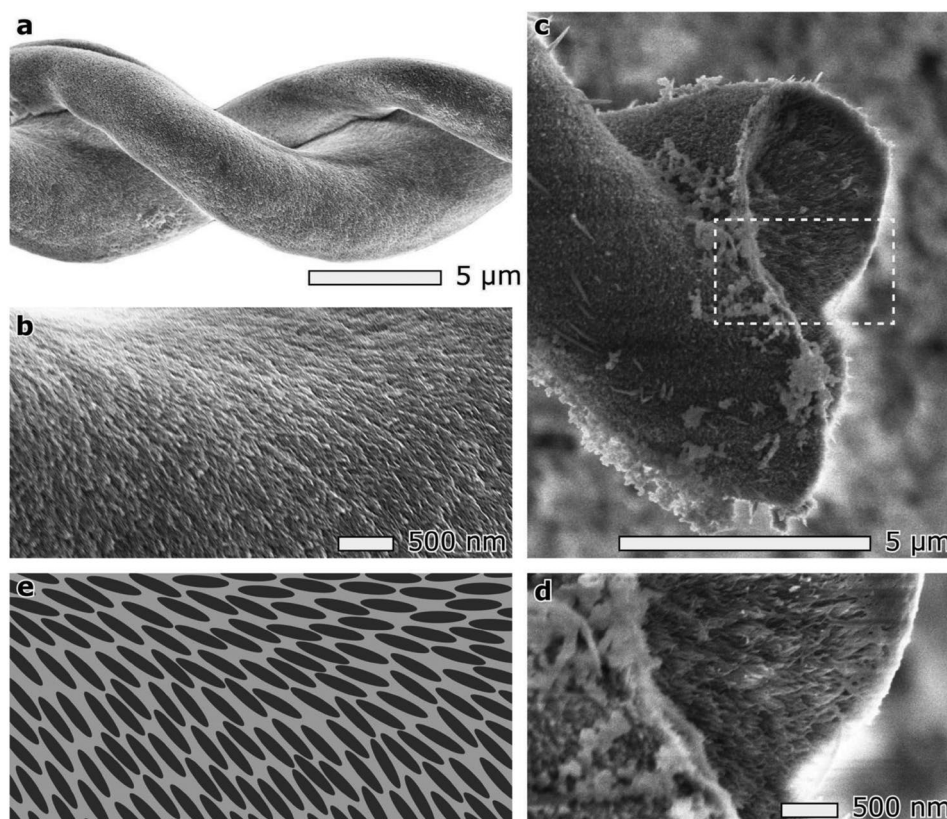


Figure 1. Visualization of the hierarchical organization of BaCO₃/SiO₂ helices. a) Electron microscopy image of the microscale helical shape. b) The nanoscale twisting of the crystals on the outside of the helix. c) A cross-sectioned helix at higher magnification, d) showing the internal ordering of the nanocrystals. e) Schematic of the aligned nanocrystals.

The polar emission angle (Θ_E) is calculated as distance of the emission peak (r_E) from the center of the Fourier plane (Figure 2c)

$$\Theta_E = \arcsin\left(\frac{r_E}{f}\right) \quad (1)$$

where f is the focal length of the microscope objective (see Section S1.2 in the Supporting Information for derivation of Equation (1)). This enables a direct comparison of the tilt direction of the helix, as determined by SEM, with the direction of the emitted beam. Additionally, Equation (1) gives the expected emission position in the Fourier plane from the polar tilt.

We analyzed the light emission for multiple helices (Figure 2a and Section S1 (Supporting Information)). All structures show directional emission, as indicated by a well-defined spot in the Fourier plane. We define the position of the light spot as the location of maximum intensity (Figure 2c), and compare the direction of the emission with the orientation of the helices previously determined by SEM. As expected, rotating the sample led to a rotation of the spot in the Fourier plane. By combining the Fourier and SEM characterization, we found a close agreement between the emission direction ($\Theta_E = 40^\circ$ and $\Phi_E = 30^\circ$) and the orientation of the helix ($\Theta_H = 44^\circ$ and $\Phi_H = 26^\circ$) (Figure 2c).

Spot sizes were characterized in terms of the beaming half-angle (i.e., half the dispersion of the emission spot in the

Fourier plane). This was 7.5° in the polar direction (Θ) and 11.5° in the azimuthal direction (Φ) (Figure 2c). A theoretical lower boundary of the beaming half-angle determined from a wave propagation simulation was 4° for light passing through a $2 \mu\text{m}$ diameter circular aperture, which is comparable to the smallest feature of the tip of the helix (Section S1.4, Supporting Information).^[27] The experimentally found beaming half-angle is close to the theoretical limit. The microscale morphology of the helix thus determines direction and dispersion of light emission.

2.2. Analyzing Circular Birefringence

Furthermore, we analyzed the optical polarization characteristics of enantiomorphous helices. The change in polarization of light transmitted through the helices can be measured using Mueller matrix polarimetry (Figure 3a). The instrument design is based on dual continuously rotating waveplates.^[28–31] The polarization state of light incident on the sample is modulated by coupling a stationary linear polarizer to a rotating quarter-waveplate. The polarization state of light transmitted by the sample is subsequently analyzed by passing the beam through a rotating quarter-waveplate followed by a stationary polarizer. The time-dependent light intensity signal produced by the combination of polarization state generator (PSG) and polarization state analyzer (PSA) can be inverted to recover the

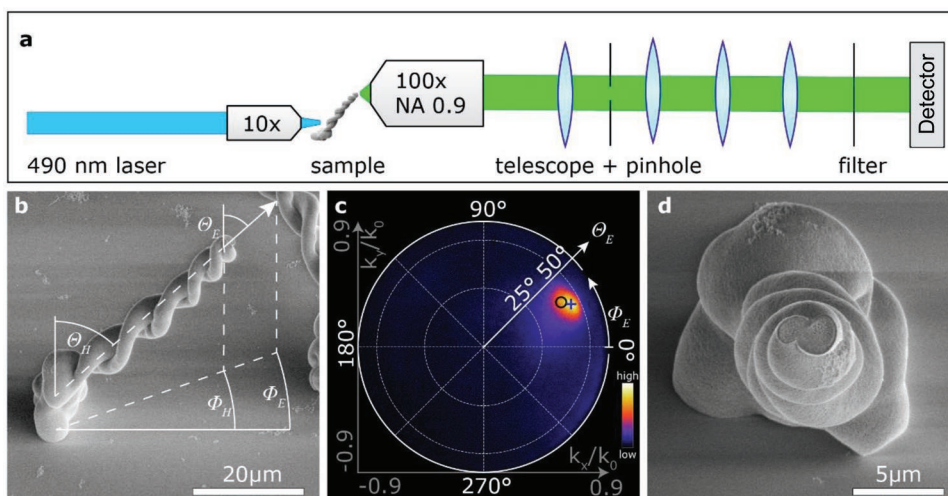


Figure 2. Directional light emission of self-assembled microhelices. a) Schematic of the Fourier microscopy setup. b) SEM image of a helix with polar tilt (Θ_H) and azimuthal rotation (Φ_H) relative to the substrate, compared with the polar angle of the emission (Θ_E) and the azimuthal rotation (Φ_E). c) The corresponding Fourier image of the emission, showing good agreement between orientation of the helix (marked with O) and the direction of the emission (marked with +) (deviation of $+4^\circ$ in Θ and -4° in Φ). The outer circle corresponds to the maximum collection angle of 64.2° as given by the objective NA of 0.9. d) Top view of the helix showing the diameter and morphology of the tip.

Mueller matrix (M), a 4×4 real-valued transformation matrix that describes the optical properties of a sample.

Light of any polarization state can be described by the Stokes vector (S), a four-element vector defined as $S = [I \ Q \ U \ V]^T$ where I is the total intensity, Q is the difference in intensity of light polarized along the x - and y -directions, U is the intensity

difference of light polarized along $\pm 45^\circ$, and V is the difference in intensity between left and right circularly polarized light. An input Stokes vector (S_{in}) can be transformed to an output Stokes vector (S_{out}) by M , so that $S_{out} = MS_{in}$.

Circular retardance (CR), the angle by which the polarization vector of light is rotated when transmitted through a sample

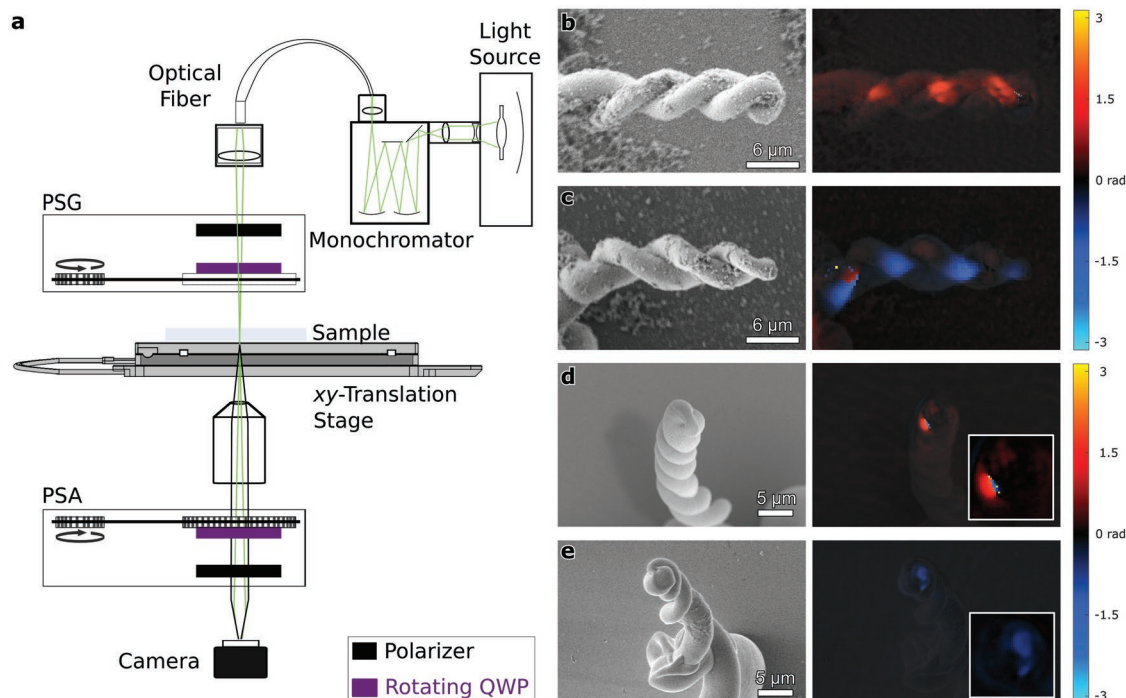


Figure 3. Circular retardance (CR) from $\text{BaCO}_3/\text{SiO}_2$ helices. a) Schematic of the Mueller matrix microscope setup. b, c) Series of electron microscopy images with CR overlaid on SEM image. A right-handed arrangement of strands (b) generates $+CR$ while a plait of opposite handedness (c) generates $-CR$. d, e) Light transmitted from the tip exhibits $+CR$ for left-handed structures (d), and $-CR$ for right-handed structures (e). Insets in (d) and (e) show a $2\times$ magnification.

(range: $\pm\pi$), can be evaluated from the differential Mueller matrix, which is approximated from the matrix logarithm (L) of M ^[28,32,33]

$$L = \begin{bmatrix} -A & -LE & -LE' & CE \\ LE & -A & CR & LR' \\ LE' & -CR & -A & -LR \\ CE & -LR' & LR & -A \end{bmatrix} \quad (2)$$

The process of obtaining L unscrambles mixed linear and circular anisotropies, providing a phenomenological understanding of the polarization transformations affected by the helices (Figure 3b–e). Although this analysis is of limited utility when encountering depolarization, it is in this case a signature of the respective enantiomorphs.^[34]

M s were measured for helices whose long axes were parallel or orthogonal with respect to the light propagation direction. Measurements were collected at normal incidence transmission for a series of helices at a wavelength of 550 nm, which lies outside of the absorption band of fluorescein (Section S2, Supporting Information). Viewed perpendicular to the helical axis, the rope-like strands of the double helix are overlaid every half period by an angle of $\approx 70^\circ$. Light propagating orthogonally through a left-handed helix, experiences a right-handed progression of anisotropic lamellae (Figure 3b) (as viewed from the detector). This generates a +CR; in other words, the incident plane of polarization is rotated clockwise (applying the normal convention for optical rotation whereby a dextrorotatory structure produces a clockwise rotation when looking at the light source). The converse is also true. In a right-handed helix, light encounters a left-handed arrangement of elements producing a levorotation (–CR) (Figure 3c). The maximum rotation in orthogonal transmission (up to 1.4 rad) was observed where the sample thickness is the greatest ($\approx 6 \mu\text{m}$).

The CR observed in Figure 3b,c can be understood from the ordering of nanocrystals within the helix, in particular the misorientation of anisotropic nanoparticles along the wave vector as it traverses the material. Skewed stacks of anisotropic lamellae are known as Reusch piles, after the scientist who used plates of mica to mimic the action of α -quartz on the azimuth of linearly polarized light passed along the optic axis.^[19,20] Dispersion theory predicts that the sense of optical rotation depends on whether the wavelength of the illumination is greater or less than the helical pitch (P) of the structure. Here, P is greater than 550 nm. Therefore, we expect that for a right-handed structure, the CR will be dextrorotary (positive) which is consistent with the experiment. The systematic dextrorotary (red) signal in the false color microscopy image of Figure 3c is likely a consequence of the inclination of this helix out of the sample plane compared with Figure 3b.

Measurements along the helical axis suffer from strong depolarization, which can be described using the degree of polarization (DOP)

$$\text{DOP} = \frac{\sqrt{Q^2 + U^2 + V^2}}{I} \quad (3)$$

The low DOP values observed are a consequence, in part, of mismatched indices of refraction between the material and its

surroundings (air); helices became dislodged when embedded in an index matching medium. Due to the low DOP, results have to be interpreted with care. Nevertheless, it is significant that the polarization responses were opposite for heterochiral helices. This provides a clue as to how the light is responding when traveling along the long axis. We presume that the helices behave as waveguides when light is transmitted through the tip; in other words, the sense of the light rotation follows the twist of the structure as in a cholesteric or twisted nematic liquid crystal.^[35] Thus, a left-handed helix (Figure 3d), which rotates the plane of polarization clockwise, operates as a dextrorotary waveguide, while a right-handed helix operates as a levorotatory waveguide (Figure 3e). Similar optical effects have been measured in twisted optical fibers, supporting the conclusion that nanocomposite helices of $\text{BaCO}_3/\text{SiO}_2$ function as waveguides.^[36,37] When subjected to an elastooptic deformation, monomode fibers generate a CR of opposite handedness to the twist. A right-handed deformation produces a levorotation.

3. Conclusion

Self-assembled, microscopic $\text{BaCO}_3/\text{SiO}_2$ double helices display directional emission and enantiomorph-specific CR. Currently, the handedness and directionality of helices are set by spontaneous symmetry breaking that occurs in the early stages of the assembly process.^[38] An exciting step forward would be to program the chirality and orientation of structures on the substrate surface by deliberately steering the assembly using top-down fabrication strategies and chiral auxiliaries.^[39,40]

In conclusion, helices emit highly directional light along their long axes, while affecting a differential refraction of left and right circularly polarized light. Normal to the helix axis, a CR is recorded that is best interpreted as a consequence of overlaid, misoriented, anisotropic lamellae. CR and directional emission originate from hierarchical ordering in helices, which intrinsically emerges from self-assembly. Overall, these results demonstrate the potential of bottom-up processes to organize simple building blocks across multiple length scales for complex functional materials.

4. Experimental Section

Growth of $\text{BaCO}_3/\text{SiO}_2$ Microhelices: Typically, 0.074 mg BaCl_2 and 0.016 g Na_2SiO_3 (Sigma-Aldrich) were dissolved in 15 mL water. The pH was adjusted to 11.2 using HCl, and 21 mg of fluorescein was added. Glass substrates of $20 \times 24 \times 1$ mm were mounted in a 100 mL beaker, and partially immersed in the growth solution before covering with a Petri dish. After 1.5 h, the glass substrates were removed and carefully rinsed with deionized water to isolate the microhelices. This procedure yielded $\approx 40 \mu\text{m}$ ensembles. These helices were found to be long enough for approximating the optical effects of multiple twists, yet robust for transport.

Geometric Analysis of Microhelices Using Scanning Electron Microscopy: The orientation of each microhelix was determined relative to the substrate using a FEI Verios 460 scanning electron microscope. The polar angle Θ_{H} was determined by orienting the sample stage such that the microhelix was parallel to the electron beam (Figure S1d, Supporting Information).

Mueller Matrix Microscopy: The Mueller Matrix (M) connects an input Stokes vector (S_{in}) to its output (S_{out}): $MS_{\text{in}} = S_{\text{out}}$. Herein, M of individual helices was measured by an imaging system based on

dual continuously rotating retarders (i.e., waveplates). The concept is explained in the Supporting Information, and the technical details of the instrument were published in full elsewhere.^[29–31]

Supporting Information

Supporting Information is available from the Wiley Online Library or from the author.

Acknowledgements

The authors would like to thank Prof. J. M. García-Ruiz for fruitful discussions. This work was part of the vernieuwingsimpuls Vidi research program “Shaping up materials” with project number 016.Vidi.189.083, which was partly financed by the Dutch Research Council (NWO). Scanning electron microscopy was partially performed at the fabrication and characterization facilities of the Amsterdam nanoCenter, supported by NWO. This work was supported secondarily by the New York University Materials Research Science and Engineering Center (MRSEC) program (Grant No. DMR-1420073). M.T. acknowledges support from The Margaret and Herman Sokol Fellowship.

Conflict of Interest

The authors declare no conflict of interest.

Keywords

bioinspired materials, hierarchical structures, optical microscopy, polarimetry, self-assembly

Received: October 4, 2019

Revised: December 7, 2019

Published online: December 23, 2019

- [1] G. M. Whitesides, B. Grzybowski, *Science* **2002**, 295, 2418.
- [2] K. Lee, W. Wagermaier, A. Masic, K. P. Kommareddy, M. Bennet, I. Manjubala, S. W. Lee, S. B. Park, H. Cölfen, P. Fratzl, *Nat. Commun.* **2012**, 3, 725.
- [3] H. Cölfen, S. Mann, *Angew. Chem., Int. Ed.* **2003**, 42, 2350.
- [4] F. Nudelman, N. A. J. M. Sommerdijk, *Angew. Chem., Int. Ed.* **2012**, 51, 6582.
- [5] A. R. Studart, *Adv. Mater.* **2012**, 24, 5024.
- [6] F. C. Meldrum, H. Cölfen, *Chem. Rev.* **2008**, 108, 4332.
- [7] The resemblance of some of these shapes with structures that were identified as microfossils, has lead García-Ruiz et al. to coin the term “biomorphs” (ref. 9,10). Note that these shapes are completely developed in the absence of organic molecules.
- [8] J. M. Garcia-Ruiz, *J. Cryst. Growth* **1985**, 73, 251.
- [9] J. M. Garcia-Ruiz, E. Melero-Garcia, S. T. Hyde, *Science* **2009**, 323, 362.
- [10] M. Kellermeier, H. Cölfen, J. M. García-Ruiz, *Eur. J. Inorg. Chem.* **2012**, 5123.
- [11] E. Bittarello, D. Aquilano, *Eur. J. Mineral.* **2007**, 19, 345.
- [12] P. Knoll, O. Steinbock, *Isr. J. Chem.* **2018**, 58, 682.
- [13] C. N. Kaplan, W. L. Noorduin, L. Li, R. Sadza, L. Folkertsma, J. Aizenberg, L. Mahadevan, *Science* **2017**, 1399, 1395.
- [14] W. L. Noorduin, A. Grinthal, L. Mahadevan, J. Aizenberg, *Science* **2013**, 340, 832.
- [15] T. Holtus, L. Helmbrecht, H. C. Hendrikse, I. Baglai, S. Meuret, G. W. P. Adhyaksa, E. C. Garnett, W. L. Noorduin, *Nat. Chem.* **2018**, 10, 740.
- [16] J. Opel, F. P. Wimmer, M. Kellermeier, H. Cölfen, *Nanoscale Horiz.* **2016**, 1, 144.
- [17] J. Opel, N. Unglaube, M. Wörner, M. Kellermeier, H. Cölfen, J. M. García-Ruiz, *Crystals* **2019**, 9, 1.
- [18] J. Opel, J. Brunner, R. Zimmermanns, T. Steegmans, E. Sturm, M. Kellermeier, H. Cölfen, J. García-Ruiz, *Adv. Funct. Mater.* **2019**, 29, 1902047.
- [19] E. Reusch, *Ann. Phys.* **1869**, 214, 628.
- [20] G. Joly, J. Billard, *J. Opt.* **1981**, 12, 323.
- [21] J. W. Anthony, R. A. Bideaux, K. W. Bladh, M. C. Nichols, *Handbook of Mineralogy*, Vol. 5, Mineral Data Publishing, Tucson, Arizona **2003**.
- [22] K. F. Lindman, *Ann. Phys.* **1920**, 368, 621.
- [23] E. D. Palik, *Handbook of Optical Constants of Solids*, Academic Press, San Diego, CA, USA **1985**.
- [24] S. Nichols, O. Arteaga, A. Martin, B. Kahr, *J. Opt. Soc. Am. A* **2015**, 32, 2049.
- [25] O. Arteaga, J. Freudenthal, B. Wang, B. Kahr, *Appl. Opt.* **2012**, 51, 6805.
- [26] A. Mohtashami, C. I. Osorio, A. F. Koenderink, *Phys. Rev. Appl.* **2015**, 4, 1.
- [27] G. Vdovin, F. van Goor, *LightPipes: Beam Propagation Toolbox*, OKO Technologies, Delft, The Netherlands **1999**.
- [28] R. M. A. Azzam, *J. Opt. Soc. Am.* **1978**, 68, 1756.
- [29] D. H. Goldstein, *Appl. Opt.* **1992**, 31, 6676.
- [30] C. Chen, I. An, G. M. Ferreira, N. J. Podraza, J. A. Zapien, R. W. Collins, *Thin Solid Films* **2004**, 455–456, 14.
- [31] S. M. Nichols, *PhD Thesis*, New York University **2017**.
- [32] J. H. Freudenthal, E. Hollis, B. Kahr, *Chirality* **2009**, 21, E20.
- [33] O. Arteaga, B. Kahr, *J. Opt. Soc. Am. B* **2019**, 36, F72.
- [34] R. Ossikovski, A. De Martino, *J. Opt. Soc. Am. A* **2015**, 32, 343.
- [35] C. V. Manguin, *Bull. Soc. Fr. Mineral.* **1911**, 34, 71.
- [36] R. Ulrich, A. Simon, *Appl. Opt.* **1979**, 18, 2241.
- [37] A. M. Smith, *Appl. Opt.* **1980**, 19, 2606.
- [38] The ratio between left- and right-handed helices during a typical experiment is close to racemic.
- [39] J. Aizenberg, D. A. Muller, J. L. Grazul, D. R. Hamann, *Science* **2003**, 299, 1205.
- [40] W. Jiang, M. S. Pacella, D. Athanasiadou, V. Nelea, H. Vali, R. M. Hazen, J. J. Gray, M. D. McKee, *Nat. Commun.* **2017**, 8, 1.